BIOCHEMISTRY
including biophysical chemistry & molecular biology

Article

pubs.acs.org/biochemistry

Recombinant Expression, Biophysical Characterization, and Cardiolipin-Induced Changes of Two *Caenorhabditis elegans* Cytochrome *c* Proteins

Amber J. Vincelli,[†] Danielle S. Pottinger,[†] Fangfang Zhong,[†] Jonas Hanske,[†,§,⊥] Stéphane G. Rolland,[‡,⊥] Barbara Conradt,[‡,⊥] and Ekaterina V. Pletneva*[,†]

[†]Department of Chemistry, Dartmouth College, Hanover, New Hampshire 03755, United States

[‡]Department of Genetics, Norris Cotton Cancer Center, Geisel School of Medicine at Dartmouth, Hanover, New Hampshire 03755, United States

[§]Department of Biology, Chemistry, and Pharmacy, Institute of Chemistry and Biochemistry, Freie Universität Berlin, D-14195 Berlin, Germany

Supporting Information

ABSTRACT: Cytochrome *c* (cyt *c*) is one of the most widely studied biomolecules, but not much is known about this protein from nematodes. Recombinant expression of *Caenorhabditis elegans* CYC-2.1 and CYC-2.2 allowed for detailed characterization of their structural features, redox properties, stabilities, and interactions with cardiolipin (CL)-containing liposomes. Using a variety of spectroscopic tools, we show that CYC-2.1 and CYC-2.2 adopt a globular α-helical fold with His/Met heme ligation. The longer CYC-2.2 has a lower thermodynamic stability than CYC-2.1 and lacks His residues to misligate to the heme in the protein's denatured state. Both *C. elegans* proteins bind to CL-containing liposomes, and these interactions promote the proteins' peroxidase activity but to a much greater degree for CYC-2.2. Dye-to-heme distance distributions from time-resolved fluorescence resonance energy transfer in bimane-labeled CYC-2.1 and CYC-2.2 revealed similar populations of extended and compact conformers for CL-bound proteins, suggesting that their distinct peroxidase activities in the presence of CL arise from differences in the local heme environments for the two polypeptide ensembles. Without inhibition from His misligation, a less stable and more prone to unfolding CYC-2.2 allows for better access of substrates to the heme and thus exhibits higher peroxidase activity. Similar features of the conformational ensembles of CYC-2.1 and CYC-2.2 to those of mammalian cyt *c* suggest that *C. elegans* proteins, particularly the former, could serve as useful models for examining the mechanism of cyt *c*−CL interactions in live organisms.

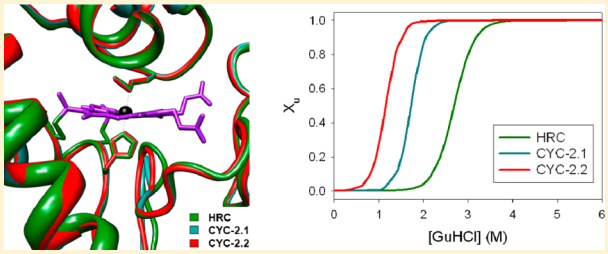

The small heme protein cytochrome *c* (cyt *c*) is one of the most widely studied biomolecules.[1,2] Since its initial characterization in the 1930s, this protein has become a major workhorse for investigations of electron transfer,[3−5] protein folding,[6−8] and macroevolution.[2] The heme prosthetic group is covalently attached to the cyt *c* polypeptide via two thioether linkages. In the native protein, endogenous His and Met amino acids occupy the two remaining coordination sites of the heme iron. Several α-helices and well-packed loops surround the heme group in a globular protein structure.[9] The protein fold, *c*-type heme linkage, and His/Met axial ligation play important roles in increasing the heme reduction potential,[10,11] allowing cyt *c* to shuttle electrons from cyt bc_1 (complex III) to cyt *c* oxidase (complex IV) within the mitochondrial intermembrane space.

In addition to its essential role in oxidative phosphorylation, new functions of cyt *c* have recently emerged.[12] The release of cyt *c* from the mitochondrial intermembrane space into the cytosol is a critical step in the execution of apoptosis.[13] In the cytosol, cyt *c* binds to apoptotic protease activating factor-1, triggering oligomerization of the latter to form the apoptosome and activating caspase cascades.[14] Interestingly, the release of cyt *c* is linked to oxidation of the mitochondrial phospholipid cardiolipin (CL), catalyzed by cyt *c* itself.[15] Interactions of cyt *c* with CL cause the protein to unfold, thereby enhancing its peroxidase activity.[16−18] This subject has become a topic of intense scientific interest and stimulated creative studies of associated changes in cyt *c* structure,[16,19] membrane morphology,[20] and cellular effects.[15,21]

With numerous successes in optical characterization of the cyt *c*−CL interactions in vitro, the next logical step is to determine their relevance in vivo. Because of its optical properties, its ease of handling, and the availability of genetic tools, the nematode *Caenorhabditis elegans* is a particularly

Received: November 2, 2012
Revised: December 31, 2012
Published: January 2, 2013

   dx.doi.org/10.1021/bi3014938 | *Biochemistry* 2013, 52, 653−666

attractive target for such investigations.[22,23] As seen in vertebrates, the outer mitochondrial membrane becomes permeable[24,25] and mitochondria fragment in a caspase-independent manner in cells that undergo apoptosis in *C. elegans*.[26] While the involvement of cyt *c* in invertebrate apoptosis has been controversial,[27,28] recent studies have firmly established an essential role of CL for *C. elegans*[29] and suggested the relevance of oxidative stress for premature apoptosis in this organism.[30] Regardless of whether cyt *c* is involved in the assembly of the *C. elegans* apoptosome, the organism could serve as a powerful platform for examining CL-induced cyt *c* conformational changes in vivo and thus providing insights into the peroxidase function of cyt *c* in the early stages of mammalian apoptosis.

Like *Saccharomyces cerevisiae*[31] and *Drosophila melanogaster*,[32] *C. elegans* possesses two cyt *c* genes, *cyc-2.1* and *cyc-2.2*.[33] Surprisingly, information about the encoded proteins CYC-2.1 and CYC-2.2 is very limited. Prior to our work, only one biochemical study has been reported, in which CYC-2.1 was isolated from *C. elegans* primarily to deduce the protein amino acid sequence.[34] The small quantities of protein that are recovered from this nematode have likely been an obstacle to detailed protein characterization. No work has been done on CYC-2.2, the protein only identified from the analysis of the *C. elegans* genome.[33]

Herein, we report structural features and redox properties of the two *C. elegans* cyt *c* proteins, CYC-2.1 and CYC-2.2, and characterize their interactions with CL-containing liposomes. We show that, similar to the well-characterized mammalian cyt *c* from horse heart (HRC), the *C. elegans* proteins adopt a globular α-helical fold with His/Met coordination of the heme iron. While the heme ligands and reduction potentials of CYC-2.1 and CYC-2.2 are alike, CYC-2.2 exhibits a much greater enhancement of peroxidase activity in the presence of CL. As in HRC,[18] analyses of time-resolved fluorescence resonance energy transfer (TR-FRET) in dye-labeled variants of CYC-2.1 and CYC-2.2 have revealed the coexistence of compact and extended CL-bound protein species. The two populations are hallmarks of CL-bound cyt *c* in vitro, with partitioning between the compact and extended species relating to the protein peroxidase activity.[18,35] Taken together, our results suggest that CYC-2.1 and CYC-2.2 are good models for examining the general mechanism of cyt *c*−CL interactions, with possible extension to studies of cyt *c* conformational dynamics in vivo.

MATERIALS AND METHODS

Tertiary Structural Predictions. Tertiary structural predictions were performed by threading the primary amino acid sequences of CYC-2.1 (NCBI entry CCD68708) or CYC-2.2 (NCBI entry CAA98555) onto the known crystal structure of the highest-scoring hidden Markov model (HMM) using the Phyre2 recognition engine.[36] CYC-2.1 aligned the best with cyt c_2 from *Rhodopila globiformis* [Protein Data Bank (PDB) entry 1HRO],[37] while CYC-2.2 aligned with the soluble segment of cyt c_{552} from *Paracoccus denitrificans* (PDB entry 3M97).[38] Structures were overlaid using the MatchMaker tool of UCSF Chimera (version 1.6.1) for comparisons.[39]

Protein Expression and Purification. Horse heart cyt *c* (HRC, Sigma catalog no. C2506) was dissolved in a 10 mM sodium phosphate buffer (pH 7.0), oxidized by the addition of solid potassium ferricyanide, and purified on a HiTrap SP HP cation exchange column (GE Healthcare) connected to an ÄKTA purifier fast protein liquid chromatography (FPLC) system as described previously.[18] The Soret band extinction coefficient (ε_{410} = 106100 M^{-1} cm^{-1}) was used to determine the protein concentration of HRC solutions.[40]

The *cyc-2.1* (NCBI entry NP_500629) and *cyc-2.2* (NCBI entry NP_506156) genes were cloned into the pET-20b(+) plasmid (Amp^R, Novagen) following the *pelB* leader sequence for periplasmic protein localization. With these plasmids, co-expression of *Escherichia coli* cyt *c* maturation proteins CcmA−H from pEC86 (Chl^R) was intended to assist with attachment of the *c*-type heme group.[41] While the dual-plasmid expression system yielded large quantities of CYC-2.1, it was not successful for CYC-2.2. Therefore, the *cyc-2.2* gene was instead inserted into the pBTR plasmid, which has been used successfully for HRC expression.[42] The *c*-type heme insertion in pBTR is accomplished with the help of yeast heme lyase, encoded in the same plasmid.[42,43] Site-directed mutations (insertion of stop codons, adjustments of cloning sites, and introduction of Cys mutations at the proteins' C-termini) were performed using protocols outlined in the QuikChange kit manual with XL1-Blue competent cells (Agilent Technologies). All plasmid sequences were verified at the Molecular Biology and Proteomics Core Facility (Dartmouth College).

Protein expression and purification were initially performed as described previously[44] and subsequently optimized as follows. The pET-20b(+) plasmid containing the *cyc-2.1* gene was cotransformed with pEC86[41] into BL21 Star (DE3) *E. coli* cells (Invitrogen), and colonies were grown on LB agar culture plates with 150−250 μg/mL carbenicillin and 34−68 μg/mL chloramphenicol at 37 °C. Colonies were screened for CYC-2.1 expression by inoculating each of twenty 7 mL cultures of Terrific Broth (TB) medium (BD Co.), containing 150 μg/mL carbenicillin and 68 μg/mL chloramphenicol, with a single isolated colony and growing the cultures at 37 °C and 220 rpm. Culture pellets were visually inspected after 6 h for the appearance of a red color, indicating recombinantly expressed heme protein. The culture with the highest level of expression was used to create a frozen stock for future use. Frozen cells were streaked onto an LB agar culture plate with 250 μg/mL carbenicillin and 68 μg/mL chloramphenicol and incubated overnight at 37 °C. Two single isolated colonies were picked into each of two 7 mL starter cultures of TB medium containing 150 μg/mL carbenicillin and 68 μg/mL chloramphenicol and grown at 37 °C and 220 rpm for 6 h. The culture pellet exhibiting the darkest red color was used to inoculate 6 L of TB medium, containing 150 μg/mL carbenicillin and 68 μg/mL chloramphenicol, for large-scale growth. The cultures were shaken at 37 °C and 220 rpm until a red pellet was observed in centrifuged 1 mL culture test samples. The cells were harvested by centrifugation (25 min at 4 °C and 4500*g*). Cell pellets were resuspended in a 50 mM Tris-HCl buffer (pH 7.5) and then frozen at −80 °C for future lysis.

The pBTR plasmid containing the *cyc-2.2* gene (Amp^R) was transformed into BL21 Star (DE3) *E. coli* cells (Invitrogen), and colonies were grown on LB agar culture plates with 100 μg/mL ampicillin at 37 °C. Frozen stocks and starter cultures for CYC-2.2 were unsuccessful. Instead, six isolated colonies were picked for direct inoculation of six 1 L cultures of TB medium, containing 100 μg/mL ampicillin, for large-scale growth. Flasks were shaken at 37 °C and 220 rpm for approximately 24 h until a red pellet was observed in centrifuged 1 mL culture test samples, and then the cells were harvested by centrifugation, resuspended in a 50 mM Tris-HCl buffer (pH 7.5), and frozen.

Frozen cell pellets were thawed on a rocker for 45 min with 1 mM phenylmethanesulfonyl fluoride (MP Biomedicals),

0.033 mg/mL DNase (Sigma-Aldrich), and approximately 0.1 mg/mL lysozyme (MP Biomedicals). The cells were lysed with a French press at 1500 psi and 4 °C to release the protein, and then the lysate was centrifuged (40 min at 4 °C and 43500*g*). The supernatant was treated with solid ammonium sulfate (351 g of salt/L of supernatant, added slowly while the solution was being stirred at 4 °C) to precipitate nontarget proteins,[45] and then the solution was centrifuged (30 min at 4 °C and 43500*g*). The supernatant was dialyzed into distilled water, followed by dialysis into a 10 mM sodium phosphate buffer (pH 7.0). Dialyzed protein was concentrated to <40 mL, oxidized by the addition of solid potassium ferricyanide, and purified on a HiLoad 26/10 SP Sepharose HP column (GE Healthcare) via FPLC.

An absorption band at ~650 nm (Figure S1 of the Supporting Information) was present in some preparations of the recombinant CYC-2.1 and CYC-2.2 proteins. The contamination giving rise to this band was successfully removed by acidic acetone treatment.[46] After addition of acidic acetone, the protein solution was gently swirled for 5 min. A 100 mM sodium borate buffer (pH 10.5) was used to resuspend the precipitated protein. The resuspended protein was dialyzed overnight against a 10 mM sodium phosphate buffer (pH 7.0) and repurified on a HiTrap SP HP cation exchange column.

The C-terminal cysteine mutants of CYC-2.1 (Leu105Cys) and CYC-2.2 (Ala107Cys)[a] were labeled with bimane iodoacetamide (Sigma-Aldrich) as previously described.[35] To prevent overlabeling, the reaction was quenched after 5 h via addition of an excess of the reducing agent dithiothreitol. The labeled variants were purified on a 5 mL HiTrap SP HP column using the same buffers that were used for wild-type proteins.

Matrix-assisted laser desorption ionization time-of-flight (MALDI-TOF) mass spectrometry measurements (Dartmouth College Molecular Biology Core Facility, Applied Biosystems Voyager-DE PRO BioSpectrometry Workstation) routinely confirmed expected masses of purified wild-type proteins and labeled variants. Protein samples were diluted to ~1 pmol/μL in 1% trifluoroacetic acid and analyzed after cocrystallization with a sinapinic acid matrix. Several samples were also examined by electrospray and Fourier transform ion cyclotron resonance (FT-ICR) mass spectrometry at the W. M. Keck Foundation Biotechnology Resource Laboratory (Yale University, New Haven, CT).

Spectroscopic Measurements. All spectroscopic experiments were conducted at 21 ± 2 °C except the low-temperature electron paramagnetic resonance (EPR) measurements. Absorption spectra associated with the 695 nm charge transfer band were measured with a JASCO V-630 scanning spectrophotometer. All other absorption and circular dichroism (CD) spectra were recorded with an Agilent 8453 diode array spectrophotometer and a JASCO J-715 spectropolarimeter, respectively. Fluorescence spectra were recorded with a HORIBA Jobin Yvon Fluorolog-3 spectrofluorometer; the intrinsic Trp and extrinsic bimane fluorophores were excited at 295 and 386 nm, respectively. All absorption and CD spectra were referenced against corresponding blanks, and Raman scattering in all fluorescence spectra was removed by subtracting spectra of the appropriate blanks.

Protein concentrations were determined spectroscopically using extinction coefficients recovered with pyridine hemochrome assays.[47] The assays were conducted in triplicate, and the concentration C (in millimolar) of heme in the pyridine solution was determined according to eq 1, which included a correction for baseline drift:[48]

$$C = \frac{1}{\varepsilon}(\Delta A_{550-750,\mathrm{II}} - \Delta A_{550-750,\mathrm{III}}) - (\Delta A_{535-750,\mathrm{II}} - \Delta A_{535-750,\mathrm{III}}) \quad (1)$$

where A is the absorbance, II and III refer to the ferrous and ferric pyridine spectra at the specified wavelengths, respectively, and ε is the pyridine hemochrome c double-difference extinction coefficient of 23.97 mM^{-1} cm^{-1} used to calculate the protein concentration.[49] Calculated protein concentrations were used to assign extinction coefficients to the spectra recorded in buffer only.

Resonance Raman spectra were acquired on a WITec confocal Raman microscope 200 with linear polarization using a 514 nm laser (spectral center of 1430, grating of 1800 grooves/mm). A 5 μL sample [concentrations between 0.5 and 1 mM, in 100 mM sodium phosphate buffer (pH 7.4)] was suspended upside-down from a coverslip over a 1.75 mm deep depression slide to create a "hanging drop" for measurements. Spectra were referenced to the spectrum of a saturated sodium salicylate[50] standard by assigning sequential pixel numbers to the output wavenumbers of the salicylate and then generating a third-order polynomial fit to the literature-reported wavenumbers at the peak intensities as a function of the pixel numbers assigned to the experimental intensity peaks. The fit equation was applied to all assigned pixel numbers of the spectrum, thereby generating referenced wavenumbers for all intensities that were used for comparison of the data.

EPR spectra were collected on a Bruker EMX 300 X-band EPR spectrometer equipped with an Air Products low-temperature liquid helium system. To obtain spectra of the heme iron, samples of ferric cyt c in a 100 mM sodium phosphate buffer (pH 7.4) were cooled to 10 ± 2 K prior to measurements. Instrument parameters were as follows: microwave frequency of 9.477 ± 0.0014 GHz, microwave power of 3.204 mW, and eight scans per sample.

TR-FRET Measurements and Analyses. Fluorescence lifetimes were measured by time-correlated single-photon counting (TCSPC) at 5000−10000 counts using a NanoLED-375L diode laser (λ_{ex} = 375 nm, <70 ps pulse width) as the excitation source and a fast TBX-04 detector. All measurements were taken under magic angle conditions. Bimane emission was monitored at 480 nm.

TR-FRET data were analyzed in MATLAB (MathWorks) by performing numerical inversion of the Laplace transform based on a set of logarithmically spaced fluorescence decay rate constants, k, as previously described.[18] The Förster relation (eq 2) allowed for the transformation of the distributions of rate constants k, $P(k)$, into distributions of donor (D)−acceptor (A) distances r, $P(r)$:[51]

$$k = k_0\left[1 + \left(\frac{R_0}{r}\right)^6\right] \quad (2)$$

where k_0 (10.8×10^7 s^{-1}) is the fluorescence decay rate of the bimane model compound, bimane-labeled *N*-acetyl-Cys, and R_0 (35 Å) is the Förster distance for the bimane−heme pair.[35]

Redox Titrations. Reduction potentials were determined following a standard spectrophotometric procedure in which cyt c was oxidized or reduced with ferri- or ferrocyanide and the absorbance at 550 nm was measured as a function of different ratios of ferri- to ferrocyanide.[52] Slopes of the linear fit of these

dependencies (Figure S2 of the Supporting Information) were used to calculate the cyt *c* reduction potentials.

Liposome Preparation Centrifugation Binding Assays. Lipids 1,1′,2,2′-tetraoleoyl cardiolipin (TOCL) and 1,2-dioleoyl-*sn*-glycero-3-phosphocholine (DOPC) (Avanti Polar Lipids, Inc.) were used to prepare a 2.2 mM liposome solution by extrusion.[35] Briefly, a chloroform-suspended DOPC/TOCL mixture in a 1:1 molar ratio was desiccated under a stream of nitrogen gas and resuspended in a 25 mM HEPES buffer (pH 7.4) to a final lipid concentration of 2.2 mM. The solution was first incubated in a shaker for 30 min at 37 °C and 220 rpm, then placed in a sonication water bath for no more than 60 min, and finally passed 11 times through a 0.1 μm (SPI) membrane filter at 50 °C using a liposome extruder (Eastern Scientific) to yield unilamellar vesicles with 40 nm radii. Vesicle sizes were analyzed at room temperature by dynamic light scattering measurements with a DynaPro NanoStar (Wyatt Technology Europe GmbH).

Centrifugation Binding Assays. Protein−liposome ultracentrifugation binding assays were performed as previously described.[18,35]

Peroxidase Assays. Intrinsic peroxidase activities (without liposomes) were measured as oxidation of guaiacol (Sigma-Aldrich) to tetraguaiacol, which absorbs strongly at 470 nm. A volume of 900 μL of cyt *c* protein in a 25 mM HEPES buffer (pH 7.4) was added to a 1 mL cuvette containing 80 μL of freshly prepared guaiacol and 20 μL of hydrogen peroxide to final concentrations of 0.94 ± 0.05 μM protein and 10 mM guaiacol. Hydrogen peroxide (H_2O_2) concentrations were varied from 0 to 75 mM and verified spectroscopically (ε_{240} = 43.6 M^{-1} cm^{-1}).[53] The solution was quickly mixed by pipeting, and the measurement was immediately begun. Tetraguaiacol (ε_{470} = 26600 M^{-1} cm^{-1}) is a product of four oxidation reactions,[54] and its formation was monitored every second for 10 min by absorbance measurements.

Another peroxidase activity assay, at a much lower H_2O_2 concentration (100 μM), was used as a control to verify that the differences in intrinsic activities of the three proteins were not related to possible artifacts from high concentrations of H_2O_2 in the guaiacol assays. The formation of etoposide phenoxyl radicals[55] catalyzed by cyt *c* was monitored by EPR spectroscopy. Protein solutions (3 μM) in a 25 mM HEPES buffer (pH 7.4) were incubated with etoposide (100 μM) for 1 h before the reaction was initiated by the addition of H_2O_2 (100 μM). No reaction was noted in the absence of cyt *c*. Samples were transferred quickly to capillary tubes (1.5 mm × 90 mm), and the first spectrum was recorded immediately afterward. Instrument parameters were as follows: 3520 G center field, 100 kHz modulation frequency, and 10.11 mW microwave power. After baseline correction, the first-derivative output of the spectrometer was integrated to give the absorbance signal and then integrated again to give the area representative of the amount of etoposide phenoxyl radical.

Peroxidase activity assays in the presence of liposomes were performed with guaiacol, as described above, except that H_2O_2 concentrations were 5 mM and lipid concentrations were varied from 0 to 200 μM. Cyt *c* solutions were mixed with freshly prepared liposome solutions in a 1:9 (v/v) ratio to prevent potential protein aggregation upon contact with lipids, and the mixtures were incubated for at least 30 min at room temperature prior to being used. The fluorescence of the native Trp residue was measured in these samples (λ_{ex} = 295 nm) to probe for unfolding behavior before the samples were added to the guaiacol/hydrogen peroxide solutions; protein concentrations were 1.07 ± 0.03 and 0.96 ± 0.03 μM during fluorescence measurements and peroxidase activity assays, respectively. Peroxidase activities were measured by the absorbance at 470 nm every second for 30 min. Linear portions of the peroxidase activity curves, indicative of the steady-state phase of tetraguaiacol formation, were fit to a first-order polynomial equation, and slopes were used to calculate the rate of tetraguaiacol formation. The dependence of the reaction rate on H_2O_2 concentration was fit to the Michaelis−Menten equation (eq 3).

$$\text{rate} = \frac{k_{cat}[H_2O_2][cyt]}{K_m^{H_2O_2} + [H_2O_2]} \tag{3}$$

Equilibrium Unfolding. Equilibrium unfolding curves were obtained from absorption, CD, and Trp fluorescence spectroscopic measurements, as previously described.[44] Protein concentrations were between 4 and 10 μM. Concentrations of guanidine hydrochloride (GuHCl, Ultrapure, MP Biomedicals) solutions were checked for accuracy with refractive index measurements[56] using an AO Scientific Instrument ABBE Mark II Digital Refractometer. Raw data curves were fit to eq 4:[57]

$$f([D]) = \left(b_f + m_f[D] + \left\{(b_u + m_u[D]) \times \exp\left[\frac{m_D([D] - [D]_{1/2})}{RT}\right]\right\}\right) \Big/ \left\{1 + \exp\left[\frac{m_D([D] - [D]_{1/2})}{RT}\right]\right\} \tag{4}$$

where [D] is the GuHCl concentration, b_f and b_u are the intercepts of the baselines in the absence of denaturant for the folded and unfolded proteins, respectively, m_f and m_u are the slopes of the respective baselines, m_D is the slope of the unfolding transition, $[D]_{1/2}$ is the GuHCl concentration at the midpoint of the unfolding transition, *R* is the ideal gas constant in joules per mole per kelvin, and *T* is the temperature in kelvin. Equation 5 was used to determine the fraction of unfolded protein (X_u) for each data point:

$$X_u = [y - (b_f + m_f[D])]/[(b_u + m_u[D]) - (b_f + m_f[D])] \tag{5}$$

where *y* is the raw data value (absorption, ellipticity, or fluorescence), [D] is the GuHCl concentration at the raw data *y* value, and m_f, b_f, m_u, and b_u were obtained from eq 4. A linear extrapolation model was used to calculate the Gibbs free energy of folding, ΔG_f°, according to eq 6:

$$-\Delta G_f^\circ = [D]_{1/2} m_D \tag{6}$$

RESULTS

Analyses of the Amino Acid Sequences. The primary coding amino acid sequences of CYC-2.1 and CYC-2.2 are 83% identical (92% similar) to each other based on NCBI BLASTp results, with the main exception being 10 additional amino acids at the N-terminus of CYC-2.2 (Figure 1A). The CYC-2.1 and CYC-2.2 protein sequences were 62% (74%) and 60% (76%) identical (similar), respectively, to that of HRC. The sequence

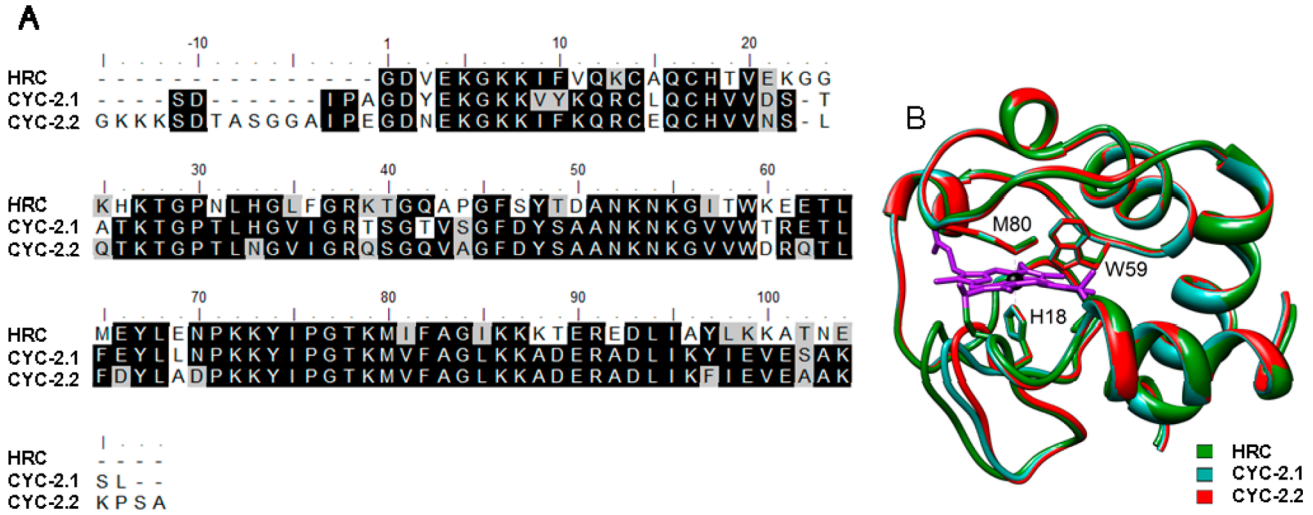

Figure 1. (A) Amino acid sequence alignment of HRC with *C. elegans* CYC-2.1 and CYC-2.2. Shaded residues indicate regions of conservation. (B) Three-dimensional structure of HRC from X-ray crystallography[9] as well as predicted structures of *C. elegans* cyt *c* proteins CYC-2.1 and CYC-2.2, created by threading their primary amino acid sequences onto the known crystal structures of the highest-ranking hidden Markov model homologues. Only polypeptide regions that overlapped with templates were predicted.

alignment (Figure 1A) revealed conservation of the HRC residues His18 and Met80 that coordinate to the heme iron in the native state, as well as residues Cys14 and Cys17 that form the thioether bonds to the porphyrin ring.[9]

A longer N-terminus is a notable feature of the CYC-2.2 sequence. A BLASTp search of the 15 N-terminal residues of this protein (GKKKSDTASGGAIPE) revealed the highest level of conservation (93% identical) with the N-termini from the hypothetical cyt *c* proteins of the sister taxa *Caenorhabditis remanei* and *Caenorhabditis briggsae*. No additional organisms were found to contain this polypeptide motif within the first 50 amino acids with at least 70% coverage. Additionally, this motif was not predicted as a signal sequence on the basis of the SignalP 4.0 Server algorithm.[58] Within the *C. elegans* proteome, no significant homology was found with this motif.

Known crystal structures[37,38] were used as templates to generate tertiary structure models of the two *C. elegans* proteins (Figure 1B). Overlaid structures illustrate general similarities of the protein folds to that of HRC but also highlight a particular region of difference located in a loop proximal to the heme (HRC residues Gly24−Asn31). This region in the *C. elegans* proteins has a gap corresponding to the critical residue His26 in HRC and cyt *c* proteins from other organisms. This residue has been implicated in the refolding and apoptotic trigger mechanisms of HRC.[17,45,59]

Expression and Characterization of Recombinant Proteins. Protein expression and purification protocols developed in this study yielded 4−5 mg of pure *C. elegans* cyt *c* proteins/L of *E. coli* culture. Mass spectrometry analyses revealed the expected masses of the proteins (Table 1). A previous report of CYC-2.1 isolated from *C. elegans* found the N-terminal Ser residue to be acetylated,[34] like HRC.[42] Not surprisingly for *E. coli* expression systems,[42] neither recombinant CYC-2.1 nor CYC-2.2 possessed this post-translational modification. This lack of an acetyl group is not expected to have a significant impact on the properties of the proteins presented in this paper.[42]

Despite numerous trials, expression of CYC-2.2 with a generally more promiscuous *E. coli* heme maturation cassette (genes *ccmA−H* within pEC86)[60] was not successful. However, insertion of the *cyc-2.2* gene into expression vector pBTR

Table 1. Molecular Masses and UV−Visible Extinction Coefficients of Recombinant *C. elegans* Cyt *c* Proteins

	mass (Da)		extinction coefficient[a] (mM^{-1} cm^{-1})	
	calculated	observed[b]	$\varepsilon_{III,Soret}$ (λ)[c]	$\Delta\varepsilon_{II-III,550}$[d]
CYC-2.1	12746	12749 ± 3	113 ± 1 (409)	21.4 ± 0.2
CYC-2.2	13848	13846 ± 6	113 ± 4 (409)	20.1 ± 0.5

[a]Determined with a pyridine hemochrome assay. [b]From mass spectrometry measurements of multiple protein samples. [c]Extinction coefficient of the ferric protein at 409 nm (Soret band). [d]Difference (ferrous minus ferric) extinction coefficient of the protein at 550 nm. The $\Delta\varepsilon_{II-III,550}$ value for HRC is 18.5 mM^{-1} cm^{-1}.[40]

yielded the desired protein product. The inability to utilize starter cultures or maintain frozen stocks of recombinant *E. coli* that consistently produced CYC-2.2 suggested that this protein might be toxic to the bacteria.

Ammonium sulfate precipitation and ion exchange chromatography have been sufficient methods for purifying functional *S. cerevisiae* and HRC cyt *c* proteins from *E. coli* recombinant expression.[18,44] In some, but not all, preparations of *C. elegans* cyt *c* proteins, an unexpected absorption band was detected at ∼650 nm after these purification steps (Figure S1 of the Supporting Information). Electrospray and FT-ICR measurements on these crude samples did not reveal the presence of additional components besides the target protein. A similar absorption band has been seen by others with a different cyt *c*,[61] and its spectral characteristics are consistent with that of verdoheme cyt *c*, a species that differs only by 3 Da in mass from the native protein.[62,63] The 650 nm band did not disappear after the protein was further purified by reverse-phase chromatography but was successfully removed (Figure S1 of the Supporting Information) by acidic acetone treatment, in which cyt *c* protein was precipitated in an acidic acetone solution. Analyses of supernatants from acidic acetone treatments revealed a number of molecules consistent with products of protein degradation. The precipitated protein was resuspended in a buffer at basic pH and purified again on an ion exchange column. Acidic acetone treatment resulted in a loss of 59−76% of the total protein. Conversion of verdoheme

to an open biliverdin structure in an acidic acetone solution could be a potential mechanism of verdocyt *c* removal.[62] Rapid degradation of the isolated material hampered our further investigations of the contaminant. Because the 650 nm absorption feature was present in only some preparations, it does not appear to be an intrinsic feature of *C. elegans* cyt *c*.

A variety of tools were used to investigate the native structural characteristics of recombinantly expressed CYC-2.1 and CYC-2.2 to determine if they are generally consistent with those of the cyt *c* family of proteins, particularly the well-characterized mammalian analogue HRC. Overlap of the HRC crystal structure with models of CYC-2.1 and CYC-2.2 from sequence threading revealed a similar placement of the conserved α-helical segments (Figure 1B). In accord with these predictions, far-UV CD spectra of CYC-2.1 and CYC-2.2 (Figure S3 of the Supporting Information) showed signals consistent with the presence of α-helices. Relative to HRC and CYC-2.1, CYC-2.2 exhibited greater helical content. A secondary structure prediction algorithm[64] yielded the following percentages of protein helical structure based on the full-length primary amino acid sequences: 30, 26, and 33% for HRC, CYC-2.1, and CYC-2.2, respectively. The predicted trend reproduced the increased propensity of CYC-2.2 for forming α-helices. However, the predicted value for HRC differed significantly from data retrieved from the protein crystal structure (48% helical),[65] reflecting the complexity of real proteins, particularly ones with large cofactor groups such as heme, for structure prediction algorithms. The stronger helical signals in *C. elegans* proteins likely arise from the extended protein termini.

The UV−visible absorption spectra of ferric and ferrous *C. elegans* proteins CYC-2.1 and CYC-2.2 (Figure 2 and Table 1) are consistent with those reported for CYC-2.1 previously isolated from *C. elegans*.[34] These spectral features closely resemble those of other *c*-type cyt proteins with His/Met heme ligation.[2]

Heme Ligands. Inspection of the near-IR absorption region (Figure 2C) of the ferric proteins revealed a 695 nm charge transfer band arising from Met−heme axial coordination. The intensity of this band has been suggested to correlate with the strength of the Met−iron bond.[66] The ε_{695} values for HRC and CYC-2.1 are nearly identical (Figure 1C), while the value for CYC-2.2 protein is ~10% lower. EPR spectra of ferric CYC-2.1 and CYC-2.2 (Figure 3A) revealed features of a low-spin state of the heme iron, consistent with His/Met coordination.[2]

To confirm similarities of the heme environments in cyt *c* proteins from *C. elegans* and mammals, the ferric proteins were further analyzed by resonance Raman spectroscopy. The high-frequency region of the resonance Raman spectrum provides information about heme coordination and spin state and is a sensitive reporter of heme environment. The spectra of the three proteins (Figure 3B) are nearly identical. With 514 nm excitation, ν_{10} and ν_{30} are particularly strong markers of the heme spin state. These peaks are observed at 1638 and 1172 cm^{-1} for CYC-2.1 and 1637 and 1172 cm^{-1} for CYC-2.2, respectively, positions consistent with a low-spin heme, with His/Met ligation.[67,68]

Spectrophotometric titrations (Figure S2 of the Supporting Information) yielded reduction potentials of 251 ± 4 and 254 ± 2 mV for CYC-2.1 and CYC-2.2, respectively. These values are near that of HRC (262 ± 2 mV)[52] and are comparable to those of other cyt *c* proteins.[69−71] These findings, once again, support His/Met ligation to the heme iron.

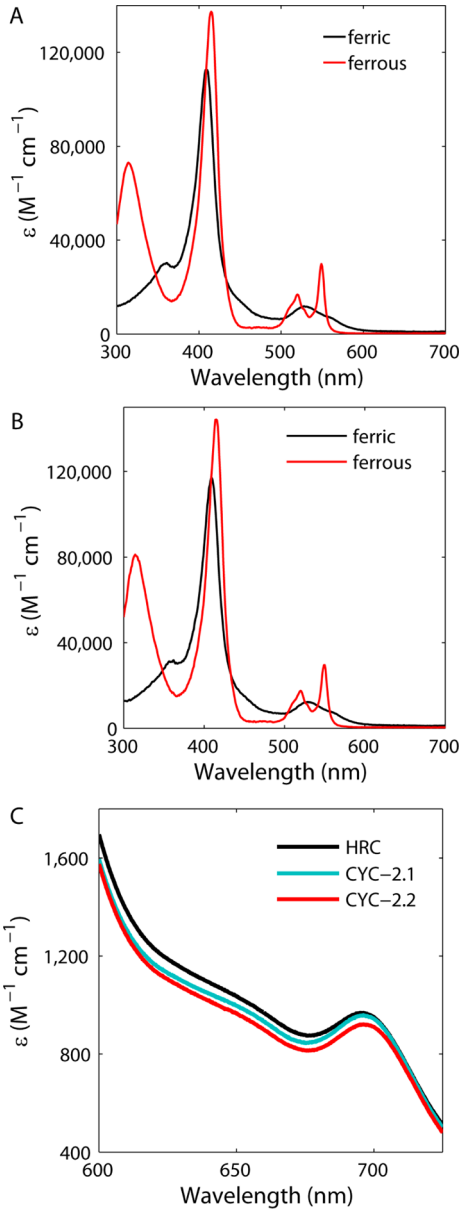

Figure 2. UV−visible absorption spectra of ferric (black) and ferrous (red) (A) CYC-2.1 and (B) CYC-2.2 at pH 7.4. Spectra of ferrous proteins include contributions to absorption signals below 350 nm from dithionite. (C) Near-IR (600−725 nm) absorption spectra of HRC, CYC-2.1, and CYC-2.2.

Intrinsic Peroxidase Activities. To further probe the heme environment in the *C. elegans* cyt *c* proteins, we conducted peroxidase assays using hydrogen peroxide (H_2O_2) and guaiacol. The guaiacol assay is a well-established procedure for investigations of peroxidase activity of cyt *c* in its native and denatured states.[72] All four previously reported phases of guaiacol oxidation were observed for HRC and *C. elegans* cyt *c* proteins over the duration of the experiment: an activation or lag phase (I), a steady-state linear phase (II), a leveling off of tetraguaiacol formation (III), and finally a degradation phase (IV).[63] Phases III and IV have been attributed to suicide inactivation of the heme catalyst and degradation of the inherently unstable tetraguaiacol product by H_2O_2.[63] HRC showed a minor peroxidase activity in the native state, and the two forms of *C. elegans* cyt *c* had greater activities than HRC at

dx.doi.org/10.1021/bi3014938 | *Biochemistry* 2013, 52, 653−666

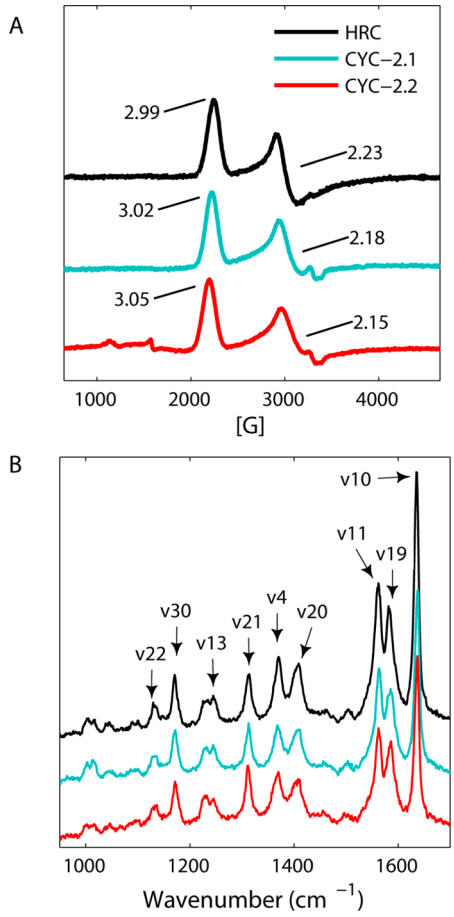

Figure 3. (A) Electron paramagnetic resonance spectra of ferric HRC (black), CYC-2.1 (cyan), and CYC-2.2 (red) proteins (450−550 μM cyt *c*) in a 100 mM sodium phosphate buffer (pH 7.4) at 10 ± 2 K. (B) Resonance Raman spectra (λ_{ex} = 514 nm) and vibrational assignments of ferric HRC (black), CYC-2.1 (cyan), and CYC-2.2 (red) proteins (0.5−1.0 mM cyt *c*) in a 100 mM sodium phosphate buffer (pH 7.4) at room temperature.

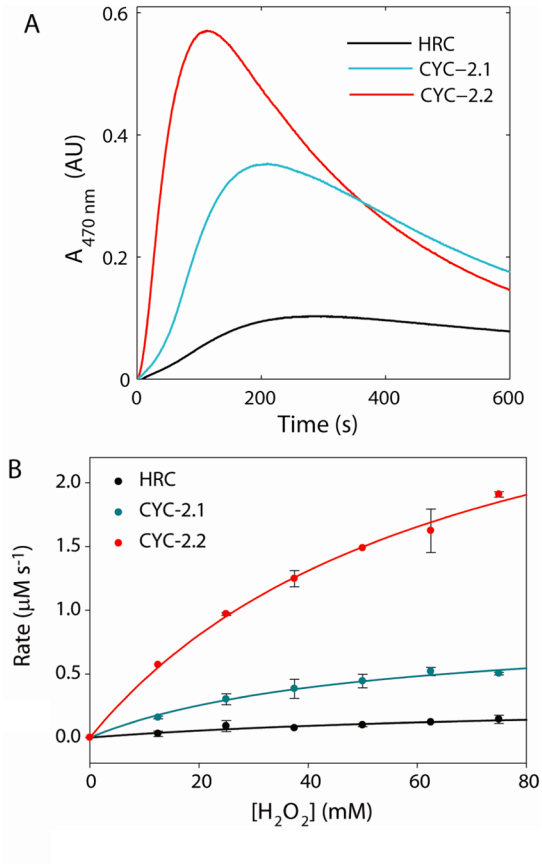

Figure 4. Peroxidase activities of HRC (black), CYC-2.1 (cyan), and CYC-2.2 (red) at pH 7.4 in a 25 mM HEPES buffer. Protein and guaiacol concentrations were 0.96 ± 0.03 μM and 10 mM, respectively. (A) Representative curves of tetraguaiacol formation (A_{470} vs time) at 50 mM H_2O_2. (B) Rates of tetraguaiacol product formation over a range of H_2O_2 concentrations. Lines are fits to eq 3 with parameters in Table 2.

Table 2. Kinetic Parameters for Guaiacol Oxidation[a]

protein	k_{cat} (s^{-1})	$K_m^{H_2O_2}$ (mM)	$k_{cat}/K_m^{H_2O_2}$ (M^{-1} s^{-1})
HRC	0.3 ± 0.1	80 ± 60	4 ± 3
CYC-2.1	0.9 ± 0.1	50 ± 10	18 ± 4
CYC-2.2	3.5 ± 0.3	70 ± 10	52 ± 8

[a]Determined from fits of the rate dependences in Figure 4B to eq 3.

a given H_2O_2 concentration [e.g., 50 mM (Figure 4A)]. Analyses of the H_2O_2 concentration dependence on the rates of guaiacol formation (Figure 4) yielded the kinetic parameters listed in Table 2. The recovered values for HRC are consistent with previous reports.[73]

The guaiacol assay has been applied to a number different cyt *c* proteins and mutants of varying thermodynamic stabilities[72,74] and thus serves as an excellent method for making direct comparisons in this work. However, this assay of a weak peroxidase cyt *c* (native protein) required high concentrations of H_2O_2, introducing the possibility of protein degradation under these conditions. A control experiment, performed by monitoring the formation of etoposide phenoxyl radicals at much lower (100 μM) concentrations of H_2O_2 catalyzed by the three cyt *c* proteins (Figure S4 of the Supporting Information), yielded the same trends as seen with guaiacol in Figure 4, arguing against artifacts from high H_2O_2 concentrations in our results.

Interactions of Protein with CL-Containing Membranes. Interactions of CYC-2.1 and CYC-2.2 proteins with CL were tested with ultracentrifugation pelleting assays and the fluorescence response from the single Trp residue in each of the two *C. elegans* proteins. Ultracentrifugation of protein−liposome solutions with increasing lipid concentrations revealed similar binding behaviors for the *C. elegans* cyt *c* proteins and HRC (Figure 5),[18] indicating no significant differences among these proteins in their binding interactions with CL-containing liposomes.

Fluorescence from the single Trp residue (Trp59 in HRC or Trp58 in CYC-2.1 and CYC-2.2) was used to probe for changes in the proteins' tertiary structures in the presence of CL (Figure 6). Trp fluorescence is quenched in the native protein by FRET to the heme.[59,75] Progressively larger amounts of CL-containing liposomes in cyt *c* solutions increased Trp fluorescence signals for all three proteins (Figure 7A), suggesting that the cyt *c*−CL interactions disrupt the proteins' tertiary structure, resulting in an increased intramolecular Trp-to-heme distance. However, even at high CL concentrations (total lipid:protein molar ratios of 200:1), the Trp signals were still smaller and their emission maxima were ∼20 nm blue-shifted, compared to signals of the GuHCl-denatured proteins. While the Trp signals in the native HRC and two *C. elegans* proteins were comparable, the magnitude

dx.doi.org/10.1021/bi3014938 | *Biochemistry* 2013, 52, 653−666

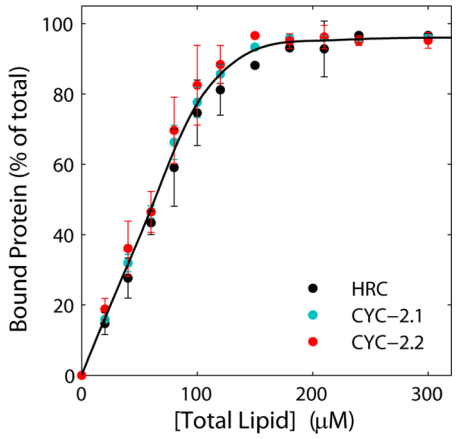

Figure 5. Percentage of cyt *c* bound to TOCL/DOPC small unilamellar vesicles (50 mol % CL, radii of 40 nm) after ultracentrifugation of protein−liposome solutions. Protein concentrations were 5 μM. The smooth curve is to guide the eye only.

of the Trp signal of CYC-2.1 was greater than that of HRC, and that of CYC-2.2 was greater than that of CYC-2.1 at each concentration of CL (Figure 7).

With the addition of CL-containing liposomes, the peroxidase activities of all three proteins increased (Figure 7B). The activity of CYC-2.2 was notably higher than the activity of either HRC or CYC-2.1. For all three proteins, no increase in peroxidase activity was detected upon addition of CL-free liposomes (Figure S5 of the Supporting Information).

Analyses of Cyt *c* Conformers by TR-FRET. C-Terminal Cys mutants of CYC-2.1 and CYC-2.2 were prepared and labeled with the small fluorophore bimane (Figure 8A). Steady-state fluorescence spectra of bimane-labeled proteins in solutions of GuHCl showed a dramatic increase in bimane fluorescence signals. Interactions of labeled CYC-2.1 and CYC-2.2 with CL-containing liposomes also increased bimane fluorescence, but to a lesser degree (Figure 8B). These results are consistent with quenching of bimane fluorescence by the heme under native conditions, when the dye and the heme are close, and a relief of the quenching when the two groups move apart upon protein unfolding.[35] No observable shifts in the bimane emission maxima from those of the native proteins were detected upon addition of CL-containing liposomes. Similar to previous results with HRC,[35] no changes in the bimane fluorescence spectra of CYC-2.1 and CYC-2.2 from those of the native proteins were observed in the presence of CL-free liposomes (Figure S5 of the Supporting Information).

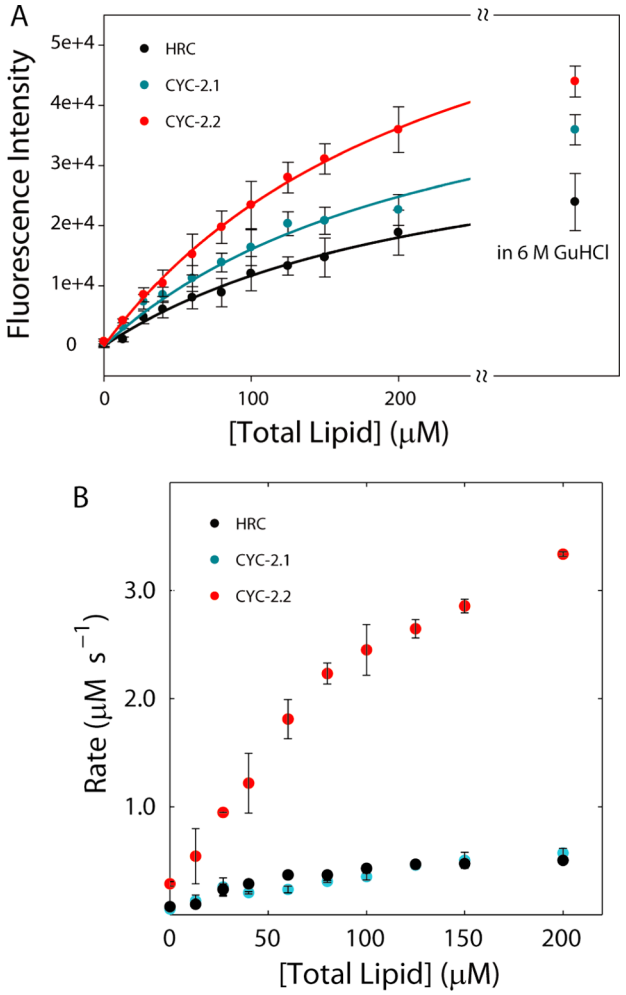

Figure 7. (A) Trp fluorescence intensities at 337 nm (λ_{ex} = 295 nm) and (B) rate constants of the linear phases of tetraguaiacol formation for HRC, CYC-2.1, and CYC-2.2 at pH 7.4 in a 25 mM HEPES buffer with various total lipid concentrations (TOCL/DOPC liposomes, 50 mol % CL). Protein concentrations were 1.07 ± 0.03 and 0.96 ± 0.03 μM during fluorescence measurements and peroxidase activity assays, respectively. In peroxidase activity assays, H_2O_2 and guaiacol concentrations were 5 and 10 mM, respectively.

TR-FRET kinetics in bimane-labeled proteins offered additional insights into the conformations of CYC-2.1 and CYC-2.2 in their native, CL-bound, and GuHCl-denatured states. These measurements revealed distinct bimane fluorescence decays

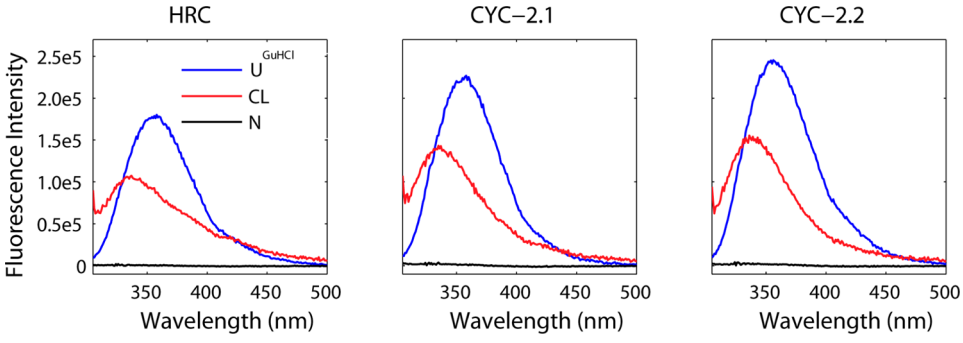

Figure 6. Fluorescence spectra (λ_{ex} = 295 nm) of 1.07 ± 0.03 μM HRC, CYC-2.1, and CYC-2.2 at pH 7.4 in a 25 mM HEPES buffer (native, black), with 6 M guanidine hydrochloride (GuHCl, blue), and with TOCL/DOPC (200 μM total lipid, 50 mol % CL) liposomes (CL, red).

dx.doi.org/10.1021/bi3014938 | *Biochemistry* 2013, 52, 653−666

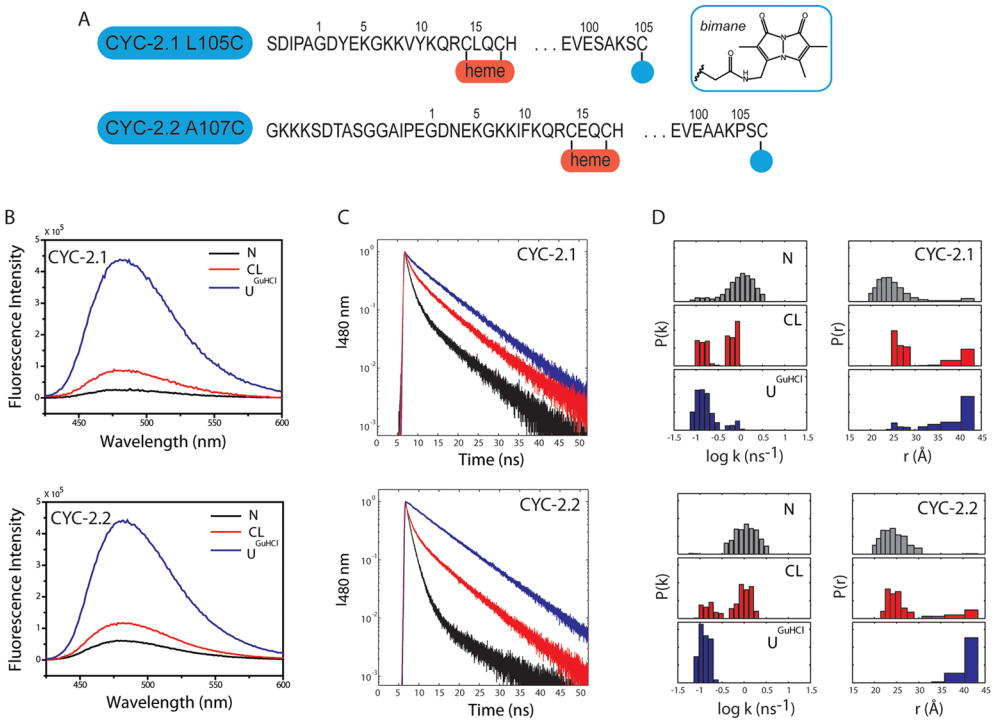

Figure 8. (A) Positions of labeling sites in CYC-2.1 and CYC-2.2 and structure of the bimane label. (B) Fluorescence spectra (λ_{ex} = 386 nm), (C) decays (λ_{ex} = 375 nm, and λ_{em} = 480 nm), and (D) distributions of rate constants $P(k)$ (left) and D−A distances $P(r)$ (right) for bimane-labeled (at Cys placed at the last residue position in each protein) CYC-2.1 and CYC-2.2 in a 25 mM HEPES buffer (pH 7.4) [native (N), gray], with TOCL/DOPC liposomes [50 mol % CL, 400 μM total lipid, CL-bound (CL), red], and in 6 M GuHCl solution at pH 7.4 [GuHCl-unfolded (U^{GuHCl}), blue]. At >43 Å distances, energy transfer rate constants and D−A distances cannot be determined reliably; the structures with $r \geq 43$ Å are represented by a single bar.

for each of these three experimental conditions (Figure 8C). Analyses of these decays yielded distributions of rate constants $P(k)$ and bimane−heme distances $P(r)$ (Figure 8D). The modes of the bimane−heme distance distributions $P(r)$ for native CYC-2.1 and CYC-2.2 were 24 ± 0.3 Å. These distances are 1−2 Å longer than bimane− and dansyl−heme distances in C-terminally labeled variants of *S. cerevisiae* iso-1 cyt *c* and HRC,[76,77] findings that are consistent with the slightly longer C-terminal helices in both *C. elegans* proteins (Figure 1A).

The decays of the GuHCl-denatured samples showed no evidence of bimane quenching, suggesting a large (≥43 Å) separation of the polypeptide N-terminus (carrying the heme group) and C-terminus (carrying the bimane group) upon unfolding of both proteins. Addition of CL-containing liposomes resulted in protein ensembles with two distinct populations of cyt *c* conformers with short (22−28 Å) and long (>30 Å) distances between bimane and heme chromophores. With the same concentration of CL-containing liposomes (400 μM total lipid, 50 mol % CL), the populations of extended conformers in CYC-2.1 and CYC-2.2 ensembles were comparable (29−43%).

Equilibrium Unfolding. Equilibrium unfolding parameters for CYC-2.1 and CYC-2.2 were obtained by monitoring protein UV−visible absorption, CD, and fluorescence spectra at increasing concentrations of GuHCl (Figure 9 and Table 3). The steep slopes of the unfolding transitions (m_D) and the similarities of the recovered parameters from all three spectroscopic methods indicated a cooperative nature of unfolding. The midpoint ($[GuHCl]_{1/2}$) of the unfolding transition for CYC-2.1 was lower than that of HRC, but the free energy of folding ΔG_f° was the same, within error, for these two proteins. The CYC-2.2 protein exhibited both a lower absolute value of ΔG_f° (at least in CD measurements) and a lower m_D than either HRC or CYC-2.1.

DISCUSSION

Characteristics of a Typical Cyt *c*. Spectroscopic measurements presented here demonstrate that both *C. elegans* proteins CYC-2.1 and CYC-2.2 have a native structure typical of cyt *c*: an α-helical fold and His/Met ligation to a *c*-type heme.[1,2] Dramatic quenching of the fluorescence emission of the sole intrinsic Trp or extrinsic bimane (placed at the proteins' C-termini) by the heme suggests a compact tertiary structure for both proteins.

Reduction potentials of ~250 mV for CYC-2.1 and CYC-2.2 fall within the range of potentials reported for cyt *c* proteins from other organisms.[69−71] This finding further confirms the similarity of the heme environments of the proteins to those of others in the cyt *c* family and hints about similar redox reactivity. The organization and function of the mitochondrial respiratory chain are alike in *C. elegans* and mammals. The genes for the *C. elegans* analogues of the cyt c_1 subunit of the cyt bc_1 complex (CYC-1) and cyt *c* oxidase subunits I (MTCE.26) and II (MTCE.31) have been identified;[33] they share >40% sequence identity with their mammalian counterparts.[78] Five of the six lysine residues known to interact with mitochondrial protein binding partners (cyt bc_1 and cyt *c* oxidase) are completely conserved (Lys8, -72, -73, -86, and -87 in HRC), with the sixth lysine (Lys13 in HRC) being an analogous, positively charged Arg in both *C. elegans* proteins. In addition, four of the six lysines implicated in peripheral interactions with binding partners (HRC residues 5, 7, 27, and 79) are also conserved.[79]

dx.doi.org/10.1021/bi3014938 | *Biochemistry* 2013, 52, 653−666

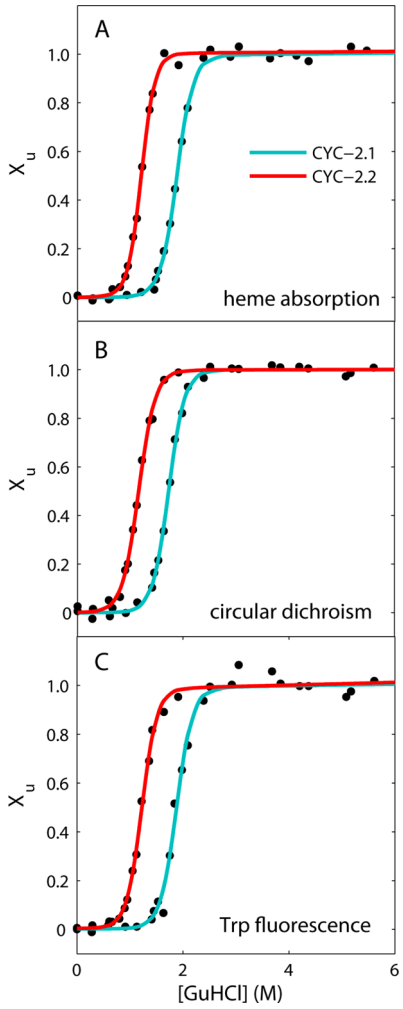

Figure 9. Equilibrium unfolding curves for the *C. elegans* cyt *c* proteins CYC-2.1 (cyan) and CYC-2.2 (red) at pH 7.4, as measured by the (A) heme absorption ratios (420 nm to 402 nm), (B) CD signals at 222 nm, and (C) Trp fluorescence intensities at 354 nm. Protein concentrations were between 4 and 10 μM. The lines represent fits to a two-state unfolding model (eq 4) with parameters in Table 3.

Thermodynamic Stability and Intrinsic Peroxidase Activity. The equilibrium unfolded studies uncovered a lower thermodynamic stability of CYC-2.2, compared to that of HRC.[18] The change in the folding Gibbs free energy (ΔG_f°) is the same, within error, for HRC and CYC-2.1, but the midpoint of the unfolding transition for CYC-2.1 is at a distinctly lower GuHCl concentration (Table 3). The errors in the calculated values of ΔG_f° arise from uncertainties in both $[\mathrm{GuHCl}]_{1/2}$ and m_D. Considering the much smaller error in the measured $[\mathrm{GuHCl}]_{1/2}$ than in m_D, the CYC-2.1 protein is likely less stable than HRC.

Two non-native His ligands, His26 and His33, misligate to the heme in HRC and contribute to stabilization of its denatured state at neutral pH.[8,59] The two *C. elegans* cyt *c* proteins both lack His26, and CYC-2.2 also has an Asn in place of His32 (His33 in HRC).[a] The N-terminal amino group could also misligate to the heme in unfolded proteins;[80] however, the blue-shifted heme absorption spectrum of CYC-2.2 in the GuHCl-denatured state (Figure S6 of the Supporting Information) suggests that this group is not a major ligand and likely does not contribute to substantial stabilization of the denatured state. With a gap in the protein sequence at position 26, misligation of the heme by His32 in CYC-2.1 yields a tighter, more destabilized polypeptide loop compared to that in the denatured HRC. This analysis argues against an increased level of stabilization of the denatured state for CYC-2.1 and CYC-2.2, compared to HRC, and instead suggests a destabilization of the native state for the *C. elegans* proteins.

Analyses of structural models for the two *C. elegans* proteins identified a number of notable differences in regions that line the heme crevice, compared to those in HRC. In addition to the sequence gap at position 26, the two bulky amino acid residues Leu35 and Ile85 (HRC numbering) are replaced by smaller Val residues ($\Delta V = -27$ Å^3) in *C. elegans* proteins. The shorter 20s–30s Ω-loop and less well-packed protein core could lead to destabilization of native CYC-2.1 and CYC-2.2, compared to HRC. Interestingly, mutations of Ile85 in *S. cerevisiae* iso-1 cyt *c* have been shown to dramatically affect the stability of this protein.[81] In CYC-2.2, the possible displacement of helices associated with the longer N- and C-termini could contribute to additional destabilization of the protein tertiary structure, despite a higher α-helical content.

The peroxidase activity of cyt *c* is a sensitive indicator of local polypeptide unfolding, which is connected to the dissociation of a fairly weak Met ligand and opening of the heme crevice. Similar to hydrogen–deuterium isotope exchange experiments, the peroxidase assay reports on the conformational fluctuations in the protein native state and offers insights about low-free energy unfolding intermediates.[72] The strong correlation between thermodynamic stability and a small (but detectable) peroxidase activity for native HRC, CYC-2.1, and CYC-2.2 (Tables 2 and 3) in this study, as well as other cyt *c* proteins,[72,74] suggests that the ease of the local polypeptide unfolding near the cyt *c* heme is related to the global stability of the protein fold.

Unfolding and Amplified Peroxidase Activities of *C. elegans* Cyt *c* Proteins upon Interactions with CL. Interactions of cyt *c* with the mitochondrion-specific lipid CL are central to protein function in both oxidative phosphorylation and apoptosis. Recent reports suggest that CL levels strongly affect

Table 3. Thermodynamic Parameters for the Unfolding Transitions of Ferric Horse Heart and *C. elegans* Cyt *c* Proteins[a]

	heme absorption[b]			circular dichroism[c]			Trp fluorescence[d]		
protein	$[\mathrm{D}]_{1/2}$ (M)	m_D (kJ mol^{-1} M^{-1})	$-\Delta G_f^\circ$ (kJ mol^{-1})	$[\mathrm{D}]_{1/2}$ (M)	m_D (kJ mol^{-1} M^{-1})	$-\Delta G_f^\circ$ (kJ mol^{-1})	$[\mathrm{D}]_{1/2}$ (M)	m_D (kJ mol^{-1} M^{-1})	$-\Delta G_f^\circ$ (kJ mol^{-1})
HRC[e]	2.60 ± 0.07	11 ± 3	29 ± 7	2.70 ± 0.06	12 ± 3	31 ± 7	2.81 ± 0.08	12 ± 4	30 ± 10
CYC-2.1	1.88 ± 0.02	16 ± 2	29 ± 4	1.72 ± 0.03	16 ± 3	28 ± 4	1.88 ± 0.06	16 ± 5	30 ± 10
CYC-2.2	1.21 ± 0.03	19 ± 3	23 ± 4	1.16 ± 0.04	16 ± 2	18 ± 3	1.22 ± 0.05	17 ± 4	21 ± 5

[a]At pH 7.4 ± 0.1 and room temperature; protein concentrations were between 4 and 10 μM. [b]Monitored at the Soret band. [c]Monitored at 222 nm. [d]Steady-state measurements of fluorescence intensity at 354 nm (λ_{ex} = 295 nm). [e]Obtained from equine heart (Sigma catalog no. C2506) and freshly purified by ion exchange chromatography before use.

dx.doi.org/10.1021/bi3014938 | *Biochemistry* 2013, 52, 653–666

C. elegans, where CL depletion causes a reduction in the mitochondrial membrane potential and abnormal mitochondrial function in germ cells.[29] There is abundant literature proposing different binding models for cyt *c*−CL interactions, with a general consensus about the importance of electrostatic interactions between the positively charged protein and the negatively charged lipid, in particular involving Lys72, -73, -86, and -87 in cyt *c*.[82,83] These four Lys residues are completely conserved in both *C. elegans* cyt *c* proteins. The same binding behavior of HRC and the two *C. elegans* proteins for binding to CL liposomes in ultracentrifugation experiments suggests the strong likelihood of a similar mode of liposome binding for all three proteins. The similar Trp emission maxima for the CL-bound proteins further support this hypothesis. Interestingly, red-shifted emission maxima of the environmentally sensitive bimane fluorophore at the C-termini of CYC-2.1 and CYC-2.2 suggest that the very end of the C-helix in these proteins is solvent-accessible and does not insert into the membrane. These findings support a predominantly peripheral binding of proteins on the liposome surface, a mechanism recently discussed for HRC.[35]

Interactions of cyt *c* with CL-rich liposome surfaces promote destabilization of the proteins' native structure and polypeptide unfolding.[16,18] Increased Trp signal intensities in the presence of CL (Figures 6 and 7A) reflect diminished levels of Trp-to-heme FRET, because of longer distances between the two chromophores. The similar shapes of the three curves (Figure 7A) are consistent with similar binding affinities of the three proteins for CL-containing liposomes. On the other hand, the magnitudes of the Trp fluorescence signal over the entire range of studied CL concentrations clearly differ among the three proteins. Analyses of the Trp fluorescence at high lipid:protein ratios, when the majority of cyt *c* is bound to CL-containing liposomes, suggest longer on average Trp-to-heme distances in the ensemble of CYC-2.1, compared to HRC, and in the ensemble of CYC-2.2, compared to CYC-2.1. These trends parallel the trends in stabilities of the three proteins ($[GuHCl]_{1/2}$) but also the trend observed for the Trp signals in denatured proteins in 6 M GuHCl (pH 7.4) (Figure 7A). Thus, the differences in the magnitude of the Trp signal could arise from differences in either the population of the unfolded species in the three protein ensembles or the degree of protein unfolding.

Measurements of TR-FRET in dye-labeled HRC revealed distinct populations of compact and extended structures for the CL-bound protein.[18,35] Herein, we identify the same behavior with bimane-labeled *C. elegans* cyt *c* proteins. Notably, these results demonstrate that under identical conditions, the CYC-2.1 and CYC-2.2 proteins have populations of extended conformers comparable to each other and to that of HRC. Scaling the signals in Figure 7A based on the magnitude of the Trp signal in GuHCl-denatured proteins yields identical Trp curves for all three proteins (Figure S7 of the Supporting Information), further supporting the similarities in the populations of the unfolded species.

While the gross features of the three ensembles of CL-bound proteins (relative populations of compact and extended conformers) appear to be the same, there are subtle conformational differences among the conformers. The magnitude of the Trp fluorescence signal is sensitive to His misligation in denatured cyt *c*, and the signals of denatured HRC, CYC-2.1, and CYC-2.2 at pH 7.4 (Figure 6) reflect the propensities for such an interaction in these proteins. With the sixth coordination site of the heme iron occupied by His33 in HRC and His32 in CYC-2.1 (a preferred non-native His ligand in HRC[59] and the only one in CYC-2.1), the peroxidase activities of these protein are lower than that of CYC-2.2. Evidently, His33 (His32) ligation, together with the surrounding polypeptide, offers similar protection to the heme in CL-bound HRC and CYC-2.1. These results corroborate earlier findings of the importance of His misligation in inhibiting the peroxidase function of denatured cyt *c*.[72]

Recent work from our laboratory has revealed interconversions between compact and extended conformers in the ensemble of CL-bound HRC.[35] These dynamics, reflected in partitioning between the two conformer types, depend on interactions of the protein with the CL-containing liposomes. In this study, we find not only similar behaviors in the binding to CL-containing liposomes for all three cyt *c* proteins but also similar distributions of compact and extended conformers from the proteins labeled with dyes at their C-termini. These findings are particularly intriguing because the proteins differ in their thermodynamic stabilities. It appears that the three cyt *c* proteins bind to the lipid surface in the same manner, with similar contacts likely provided by conserved residues. Even though cyt *c* does substantially unfold on the liposome surface, the denaturing mechanism seems to involve specific protein−lipid interactions.

The largely open, extended conformers are of particular functional importance because they are likely to exhibit the greatest peroxidase activity.[18] Distributions of distances between the heme and the protein C-terminus from TR-FRET experiments probe general features of the polypeptide ensemble. While these global features are similar for CYC-2.1 and CYC-2.2, distinct peroxidase activities highlight differences in the heme local environment among the protein conformers. Both global and local characteristics of the protein conformers are thus important considerations in the analysis of functional implications of cyt *c* unfolding.

Dual-Cyt *c* Systems. Although only one cyt *c* is generally found in mammals, encoding of two cyts *c* is not unusual. *S. cerevisiae* possesses two cyt *c* genes, *CYC1* and *CYC7*, that encode iso-1 and iso-2 cyt *c*, respectively; expression of these two genes appears to be linked to the growth conditions.[31] The fruit fly *D. melanogaster* expresses two cyt *c* analogues, cyt-*c-p* and cyt-*c-d*, that are tissue-specific: while cyt-*c-p* is mainly somatic, cyt-*c-d* is expressed almost exclusively in the male germ line. However, both *D. melanogaster* cyt *c* proteins can function interchangeably in both respiration and apoptosis.[84]

Interestingly, a second isoform of cyt *c* has also been identified in mice.[85] This testis-specific isoform, T-cyt *c*, is expressed only in the germinal epithelial cells. T-cyt *c* has a 4-fold higher apoptotic activity than the somatic protein, which was postulated to play an important role in maintaining the integrity of the sperm.[86] The testis isoform is a nontranscribed pseudogene in humans.[12]

Because of its high degree of homology to mammalian cyt *c*, CYC-2.1 has been proposed to fulfill the classic role of cyt *c* in the respiratory chain,[34] whereas the function of CYC-2.2 remains obscure. The two *C. elegans* cyt *c* proteins exhibit a high degree of homology in their core sequence, yet the N-terminus of CYC-2.2 contains a highly basic triple-lysine sequence that is not found in CYC-2.1 (Figure 1A). Gene expression maps show that both genes are expressed in different amounts of correlated genes.[87] The CYC-2.1 expression pattern seems to be correlated with germline-enriched genes and oocytes, whereas CYC-2.2 expression correlates with sperm-enriched genes and major sperm proteins, suggesting a disparate role of both paralogs in sexual reproduction.[87] It is tempting to speculate about possible

functional parallels of the two *C. elegans* cyt *c* proteins with other dual-cyt *c* systems, where one isoform plays a role in reproduction. Analysis of time- and tissue-specific expression patterns of the two proteins in *C. elegans* will test this idea in future genetics and cell biology work.

In conclusion, *C. elegans* proteins CYC-2.1 and CYC-2.2 have typical features of mitochondrial cyt *c*, namely, His/Met heme coordination, high reduction potentials, and a globular α-helical fold. The somewhat longer CYC-2.2 has a lower thermodynamic stability and higher intrinsic peroxidase activity than CYC-2.1. The two *C. elegans* cyt *c* proteins, like HRC, bind to CL-containing liposomes. This interaction promotes unfolding and enhances peroxidase activities of the proteins. Similar features of the conformational ensembles of CL-bound CYC-2.1 and CYC-2.2 compared to those of mammalian cyt *c* suggest that these *C. elegans* proteins, especially the former, could serve as useful models for in vivo fluorescence studies of interactions of cyt *c* with mitochondria.

■ ASSOCIATED CONTENT

Supporting Information

Representative near-IR absorption spectra of *C. elegans* cyt *c* proteins before and after acidic acetone treatment, determination of reduction potentials for *C. elegans* cyt *c* proteins, far-UV CD spectra of HRC and *C. elegans* cyt *c* proteins, etoposide assay of the intrinsic peroxidase activity of the three proteins, peroxidase activity and protein unfolding assays with CL-free liposomes, absorption spectra of native and GuHCl-denatured proteins at pH 4.5 and 7.4, and scaled changes in Trp fluorescence with added CL-containing liposomes. This material is available free of charge via the Internet at http://pubs.acs.org.

■ AUTHOR INFORMATION

Corresponding Author

*Phone: (603) 646-0933. E-mail: ekaterina.pletneva@dartmouth.edu.

Present Addresses

[‖]Center for Integrated Protein Science Munich (CIPSM), Department of Biology II, Ludwig Maximilians University Munich, 82152 Planegg-Martinsried, Germany.

[⊥]Max Planck Institute of Colloids and Interfaces, Department of Biomolecular Systems, Arnimalle 22, 14195 Berlin-Dahlem, Germany.

Funding

This work was funded by Dartmouth College startup funds (E.V.P.), CIPSM (B.C.), funds from the Ludwig Maximilians University Munich (B.C.), and National Institutes of Health Grants GM069950 (B.C.), GM076651 (B.C.), and GM098502 (E.V.P.). A Zabriskie Fellowship supported Senior Honors research (D.S.P.).

Notes

The authors declare no competing financial interest.

■ ACKNOWLEDGMENTS

We thank Michael Q. Zhu and Philipp B. Rentzsch for their help with protein expression and characterization of the protein contaminant, Anna M. Morenz for her preliminary work on peroxidase assays, and Kara L. Bren for the pBTR plasmid.

■ ABBREVIATIONS

cyt *c*, cytochrome *c*; HRC, horse heart cytochrome *c*; GuHCl, guanidine hydrochloride; CD, circular dichroism; CL, cardiolipin; TOCL, 1,1′,2,2′-tetraoleoyl cardiolipin; DOPC, 1,2-dioleoyl-*sn*-glycero-3-phosphocholine; TCSPC, time-correlated single-photon counting; TR-FRET, time-resolved fluorescence resonance energy transfer; FT-ICR, Fourier transform ion cyclotron resonance; MALDI-TOF, matrix-assisted laser desorption ionization time-of-flight; HMM, hidden Markov model.

■ ADDITIONAL NOTE

[a]The equine cyt *c* numbering system is used throughout the text. Because of a residue gap at position 26 in the *C. elegans* cyt *c* proteins, all residues after the gap differ by −1 from the corresponding residues in the equine sequence; e.g., Trp58 in *C. elegans* CYC-2.1 and CYC-2.2 corresponds to Trp59 in HRC.

■ REFERENCES

(1) Scott, R. A., and Mauk, A. G., Eds. (1996) *Cytochrome c: A Multidisciplinary Approach*, University Science Books, Sausalito, CA.

(2) Moore, G. R., and Pettigrew, G. W. (1990) *Cytochromes c: Evolutionary, Structural, and Physicochemical Aspects*, Springer-Verlag, New York.

(3) Wuttke, D. S., Bjerrum, M. J., Winkler, J. R., and Gray, H. B. (1992) Electron-tunneling pathways in cytochrome *c*. *Science 256*, 1007−1009.

(4) Galinato, M. G., Kleingardner, J. G., Bowman, S. E., Alp, E. E., Zhao, J., Bren, K. L., and Lehnert, N. (2012) Heme-protein vibrational couplings in cytochrome *c* provide a dynamic link that connects the heme-iron and the protein surface. *Proc. Natl. Acad. Sci. U.S.A. 109*, 8896−8900.

(5) Wei, J., Liu, H., Khoshtariya, D. E., Yamamoto, H., Dick, A., and Waldeck, D. H. (2002) Electron-transfer dynamics of cytochrome *c*: A change in the reaction mechanism with distance. *Angew. Chem., Int. Ed. 41*, 4700−4703.

(6) Maity, H., Maity, M., and Englander, S. W. (2004) How cytochrome *c* folds, and why: Submolecular foldon units and their stepwise sequential stabilization. *J. Mol. Biol. 343*, 223−233.

(7) Winkler, J. R. (2004) Cytochrome *c* folding dynamics. *Curr. Opin. Chem. Biol. 8*, 169−174.

(8) Hammack, B. N., Smith, C. R., and Bowler, B. E. (2001) Denatured state thermodynamics: Residual structure, chain stiffness, and scaling factors. *J. Mol. Biol. 311*, 1091−1104.

(9) Bushnell, G. W., Louie, G. V., and Brayer, G. D. (1990) High-resolution 3-dimensional structure of horse heart cytochrome *c*. *J. Mol. Biol. 214*, 585−595.

(10) Tezcan, F. A., Winkler, J. R., and Gray, H. B. (1998) Effects of ligation and folding on reduction potentials of heme proteins. *J. Am. Chem. Soc. 120*, 13383−13388.

(11) Mao, J., Hauser, K., and Gunner, M. R. (2003) How cytochromes with different folds control heme redox potentials. *Biochemistry 42*, 9829−9840.

(12) Hüttemann, M., Pecina, P., Rainbolt, M., Sanderson, T. H., Kagan, V. E., Samavati, L., Doan, J. W., and Lee, I. (2011) The multiple functions of cytochrome *c* and their regulation in life and death decisions of the mammalian cell: From respiration to apoptosis. *Mitochondrion 11*, 369−381.

(13) Ow, Y.-L. P., Green, D. R., Hao, Z., and Mak, T. W. (2008) Cytochrome *c*: Functions beyond respiration. *Nat. Rev. Mol. Cell Biol. 9*, 532−542.

(14) Zou, H., Li, Y., Liu, X., and Wang, X. (1999) An APAF-1·cytochrome *c* multimeric complex is a functional apoptosome that activates procaspase-9. *J. Biol. Chem. 274*, 11549−11556.

(15) Kagan, V. E., Tyurin, V. A., Jiang, J., Tyurina, Y. Y., Ritov, V. B., Amoscato, A. A., Osipov, A. N., Belikova, N. A., Kapralov, A. A., Kini, V., Vlasova, I. I., Zhao, Q., Zou, M., Di, P., Svistunenko, D. A., Kurnikov, I. V., and Borisenko, G. G. (2005) Cytochrome *c* acts as a cardiolipin oxygenase required for release of proapoptotic factors. *Nat. Chem. Biol. 1*, 223−232.

(16) Belikova, N. A., Vladimirov, Y. A., Osipov, A. N., Kapralov, A. A., Tyurin, V. A., Potapovich, M. V., Basova, L. V., Peterson, J., Kurnikov, I. V., and Kagan, V. E. (2006) Peroxidase activity and structural transitions of cytochrome *c* bound to cardiolipin-containing membranes. *Biochemistry 45*, 4998−5009.
(17) Balakrishnan, G., Hu, Y., Oyerinde, O. F., Su, J., Groves, J. T., and Spiro, T. G. (2007) A conformational switch to *β*-sheet structure in cytochrome *c* leads to heme exposure. Implications for cardiolipin peroxidation and apoptosis. *J. Am. Chem. Soc. 129*, 504−505.
(18) Hanske, J., Toffey, J. R., Morenz, A. M., Bonilla, A. J., Schiavoni, K. H., and Pletneva, E. V. (2012) Conformational properties of cardiolipin-bound cytochrome *c*. *Proc. Natl. Acad. Sci. U.S.A. 109*, 125−130.
(19) Silkstone, G., Kapetanaki, S. M., Husu, I., Vos, M. H., and Wilson, M. T. (2012) Nitric oxide binding to the cardiolipin complex of ferric cytochrome *c*. *Biochemistry 51*, 6760−6766.
(20) Beales, P. A., Bergstrom, C. L., Geerts, N., Groves, J. T., and Vanderlick, T. K. (2011) Single vesicle observations of the cardiolipin-cytochrome *c* interaction: Induction of membrane morphology changes. *Langmuir 27*, 6107−6115.
(21) Godoy, L. C., Muñoz-Pinedo, C., Castro, L., Cardaci, S., Schonhoff, C. M., King, M., Tórtora, V., Marín, M., Miao, Q., Jiang, J. F., Kapralov, A., Jemmerson, R., Silkstone, G. G., Patel, J. N., Evans, J. E., Wilson, M. T., Green, D. R., Kagan, V. E., Radi, R., and Mannick, J. B. (2009) Disruption of the M80-Fe ligation stimulates the translocation of cytochrome *c* to the cytoplasm and nucleus in nonapoptotic cells. *Proc. Natl. Acad. Sci. U.S.A. 106*, 2653−2658.
(22) Horvitz, H. R. (2003) Worms, Life, and Death (Nobel Lecture). *ChemBioChem 4*, 697−711.
(23) Conradt, B. (2009) Genetic control of programmed cell death during animal development. *Annu. Rev. Genet. 43*, 493−523.
(24) Wang, X., Yang, C., Chai, J., Shi, Y., and Xue, D. (2002) Mechanisms of AIF-mediated apoptotic DNA degradation in *Caenorhabditis elegans*. *Science 298*, 1587−1592.
(25) Parrish, J., Li, L., Klotz, K., Ledwich, D., Wang, X., and Xue, D. (2001) Mitochondrial endonuclease G is important for apoptosis in *C. elegans*. *Nature 412*, 90−94.
(26) Jagasia, R., Grote, P., Westermann, B., and Conradt, B. (2005) DRP-1-mediated mitochondrial fragmentation during EGL-1-induced cell death in *C. elegans*. *Nature 433*, 754−760.
(27) Kornbluth, S., and White, K. (2005) Apoptosis in *Drosophila*: Neither fish nor fowl (nor man, nor worm). *J. Cell Sci. 118*, 1779−1787.
(28) Martin, S. J. (2002) Destabilizing influences in apoptosis: Sowing the seeds of IAP destruction. *Cell 109*, 793−796.
(29) Sakamoto, T., Inoue, T., Otomo, Y., Yokomori, N., Ohno, M., Arai, H., and Nakagawa, Y. (2012) Deficiency of cardiolipin synthase causes abnormal mitochondrial function and morphology in germ cells of *Caenorhabditis elegans*. *J. Biol. Chem. 287*, 4590−4601.
(30) González-Cabo, P., Bolinches-Amorós, A., Cabello, J., Ros, S., Moreno, S., Baylis, H. A., Palau, F., and Vázquez-Manrique, R. P. (2011) Disruption of the ATP-binding cassette B7 (ABTM-1/ABCB7) induces oxidative stress and premature cell death in *Caenorhabditis elegans*. *J. Biol. Chem. 286*, 21304−21314.
(31) Laz, T. M., Pietras, D. F., and Sherman, F. (1984) Differential regulation of the duplicated isocytochrome *c* genes in yeast. *Proc. Natl. Acad. Sci. U.S.A. 81*, 4475−4479.
(32) Limbach, K. J., and Wu, R. (1985) Characterization of two *Drosophila melanogaster* cylochrome *c* genes and their transcripts. *Nucleic Acids Res. 13*, 631−644.
(33) *C. elegans* Sequencing Consortium (1998) Genome sequence of the nematode *C. elegans*: a platform for investigating biology. *Science 282*, 2012−2018.
(34) Vanfleteren, J. R., Evers, E. A., Van de Werken, G., and Van Beeumen, J. J. (1990) The primary structure of cytochrome *c* from the nematode *Caenorhabditis elegans*. *Biochem. J. 271*, 613−620.
(35) Hong, Y., Muenzner, J., Grimm, S. K., and Pletneva, E. V. (2012) Origin of the conformational heterogeneity of cardiolipin-bound cytochrome *c*. *J. Am. Chem. Soc. 134*, 18713−18723.
(36) Kelley, L. A., and Sternberg, M. J. E. (2009) Protein structure prediction on the Web: A case study using the Phyre server. *Nat. Protoc. 4*, 363−371.
(37) Benning, M. M., Meyer, T. E., and Holden, H. M. (1996) Molecular structure of a high potential cytochrome c_2 isolated from *Rhodopila globiformis*. *Arch. Biochem. Biophys. 333*, 338−348.
(38) Rajendran, C., Ermler, U., Ludwig, B., and Michel, H. (2010) Structure at 1.5 Å resolution of cytochrome c_{552} with its flexible linker segment, a membrane-anchored protein from *Paracoccus denitrificans*. *Acta Crystallogr. D66*, 850−854.
(39) Pettersen, E. F., Goddard, T. D., Huang, C. C., Couch, G. S., Greenblatt, D. M., Meng, E. C., and Ferrin, T. E. (2004) UCSF Chimera: A visualization system for exploratory research and analysis. *J. Comput. Chem. 25*, 1605−1612.
(40) Margoliash, E., and Frohwirt, N. (1959) Spectrum of horse-heart cytochrome *c*. *Biochem. J. 71*, 570−572.
(41) Arslan, E., Schulz, H., Zufferey, R., Künzler, P., and Thöny-Meyer, L. (1998) Overproduction of the *Bradyrhizobium japonicum c*-Type Cytochrome Subunits of the cbb_3 Oxidase in *Escherichia coli*. *Biochem. Biophys. Res. Commun. 251*, 744−747.
(42) Patel, C. N., Lind, M. C., and Pielak, G. J. (2001) Characterization of horse cytochrome *c* expressed in *Escherichia coli*. *Protein Expression Purif. 22*, 220−224.
(43) Pollock, W. B. R., Rosell, F. I., Twitchett, M. B., Dumont, M. E., and Mauk, A. G. (1998) Bacterial expression of a mitochondrial cytochrome *c*. Trimethylation of Lys72 in yeast *iso*-1 cytochrome *c* and the alkaline conformational transition. *Biochemistry 37*, 6124−6131.
(44) Pletneva, E. V., Gray, H. B., and Winkler, J. R. (2005) Many faces of the unfolded state: Conformational heterogeneity in denatured yeast cytochrome *c*. *J. Mol. Biol. 345*, 855−867.
(45) Rumbley, J. N., Hoang, L., and Englander, S. W. (2002) Recombinant equine cytochrome *c* in *Escherichia coli*: High-level expression, characterization, and folding and assembly mutants. *Biochemistry 41*, 13894−13901.
(46) Walsh, T., Johnson, M. K., Barber, D., Thomson, A. J., and Greenwood, C. (1981) Studies on heme *d*1 extracted from *Pseudomonas aeruginosa* nitrite reductase. *J. Inorg. Biochem. 14*, 15−31.
(47) Aron, J., Baldwin, D. A., Marques, H. M., Pratt, J. M., and Adams, P. A. (1986) Hemes and hemoproteins. 1: Preparation and analysis of the heme-containing octapeptide (microperoxidase-8) and identification of the monomeric form in aqueous solution. *J. Inorg. Biochem. 27*, 227−243.
(48) Yonetani, T. (1965) Studies on cytochrome c peroxidase. II. Stoichiometry between enzyme, H_2O_2, and ferrocytochrome *c* and enzymic determination of extinction coefficients of cytochrome *c*. *J. Biol. Chem. 240*, 4509−4514.
(49) Berry, E. A., and Trumpower, B. L. (1987) Simultaneous determination of hemes-*a*, hemes-*b*, and hemes-*c* from pyridine hemochrome spectra. *Anal. Biochem. 161*, 1−15.
(50) Humbert, B. (1998) Infrared and Raman spectroscopical studies of salicylic and salicylate derivatives in aqueous solution. *Spectrochim. Acta, Part A 54*, 465−476.
(51) Förster, T. (1948) Zwischenmolekulare Energiewanderung und Fluoreszenz. *Ann. Phys. (Weinheim, Ger.) 2*, 55−75.
(52) Craig, D. B., and Nichols, E. R. (2006) Spectroscopic measurement of the redox potential of cytochrome *c* for the undergraduate biochemistry laboratory. *J. Chem. Educ. 83*, 1325.
(53) Arnao, M. B., Acosta, M., del Río, J. A., Varón, R., and García-Cánovas, F. (1990) A kinetic study on the suicide inactivation of peroxidase by hydrogen peroxide. *Biochim. Biophys. Acta 1041*, 43−47.
(54) Baldwin, D. A., Helder, M. M., and Pratt, J. M. (1987) Hemes hemoproteins. 5: Kinetics of the peroxidatic activity of micro-peroxidase-8: model for the peroxidase enzymes. *J. Inorg. Biochem. 30*, 203−217.
(55) Tyurina, Y. Y., Kini, V., Tyurin, V. A., Vlasova, I. I., Jiang, J., Kapralov, A. A., Belikova, N. A., Yalowich, J. C., Kurnikov, I. V., and Kagan, V. E. (2006) Mechanisms of cardiolipin oxidation by cytochrome *c*: Relevance to pro- and antiapoptotic functions of etoposide. *Mol. Pharmacol. 70*, 706−717.

(56) Nozaki, Y. (1972) The preparation of guanidine hydrochloride. *Methods Enzymol. 26*, 43−50.
(57) Pace, N. C., Shirley, B. A., and Thomson, J. A. (1990) Measuring the Conformational Stability of a Protein. In *Protein Structure: A Practical Approach* (Creighton, T. F., Ed.) pp 311−330, IRL Press, Oxford, U.K.
(58) Petersen, T. N., Brunak, S., von Heijne, G., and Nielsen, H. (2011) SignalP 4.0: Discriminating signal peptides from transmembrane regions. *Nat. Methods 8*, 785−786.
(59) Colón, W., Wakem, L. P., Sherman, F., and Roder, H. (1997) Identification of the predominant non-native histidine ligand in unfolded cytochrome *c*. *Biochemistry 36*, 12535−12541.
(60) Kleingardner, J. G., and Bren, K. L. (2011) Comparing substrate specificity between cytochrome *c* maturation and cytochrome *c* heme lyase systems for cytochrome *c* biogenesis. *Metallomics 3*, 396−403.
(61) Hickey, D. R., Berghuis, A. M., Lafond, G., Jaeger, J. A., Cardillo, T. S., McLendon, D., Das, G., Sherman, F., Brayer, G. D., and McLendon, G. (1991) Enhanced thermodynamic stabilities of yeast iso-1-cytochromes *c* with amino acid replacements at positions 52 and 102. *J. Biol. Chem. 266*, 11686−11694.
(62) Lagarias, J. C. (1982) Bile pigment−protein interactions. Coupled oxidation of cytochrome *c*. *Biochemistry 21*, 5962−5967.
(63) Diederix, R. E., Fittipaldi, M., Worrall, J. A., Huber, M., Ubbink, M., and Canters, G. W. (2003) Kinetic stability of the peroxidase activity of unfolded cytochrome *c*: Heme degradation and catalyst inactivation by hydrogen peroxide. *Inorg. Chem. 42*, 7249−7257.
(64) Garnier, J., Gibrat, J. F., and Robson, B. (1996) GOR method for predicting protein secondary structure from amino acid sequence. *Methods Enzymol. 266*, 540−553.
(65) Serdyuk, I. N., Zaccai, N. R., and Zaccai, J. (2007) in *Methods in Molecular Biophysics*, p 553, Cambridge University Press, New York.
(66) Schejter, A., and George, P. (1964) The 695-mμ band of ferricytochrome *c* and its relationship to protein conformation. *Biochemistry 3*, 1045−1049.
(67) Hildebrandt, P., and Stockburger, M. (1986) Surface-enhanced resonance Raman spectroscopy of cytochrome *c* at room and low temperatures. *J. Phys. Chem. 90*, 6017−6024.
(68) Spiro, T. G., and Strekas, T. C. (1974) Resonance Raman spectra of heme proteins. Effects of oxidation and spin state. *J. Am. Chem. Soc. 96*, 338−345.
(69) Takamiya, S., Yu, Y., Cavaleante, M. E., Murayama, K., Taka, H., Tateno, S., Takeuchi, T., and Aoki, T. (1996) Molecular and functional properties of cytochrome *c* from adult *Ascaris suum* muscle. *Mol. Biochem. Parasitol. 79*, 61−70.
(70) Koshy, T. I., Luntz, T. L., Schejter, A., and Margoliash, E. (1990) Changing the invariant proline-30 of rat and *Drosophila melanogaster* cytochromes *c* to alanine or valine destabilizes the heme crevice more than the overall conformation. *Proc. Natl. Acad. Sci. U.S.A. 87*, 8697−8701.
(71) Guillemette, J. G., Barker, P. D., Eltis, L. D., Lo, T. P., Smith, M., Brayer, G. D., and Mauk, A. G. (1994) Analysis of the bimolecular reduction of ferricytochrome *c* by ferrocytochrome b_5 through mutagenesis and molecular modeling. *Biochimie 76*, 592−604.
(72) Diederix, R. E., Ubbink, M., and Canters, G. W. (2002) Peroxidase activity as a tool for studying the folding of *c*-type cytochromes. *Biochemistry 41*, 13067−13077.
(73) Hamachi, I., Fujita, A., and Kunitake, T. (1997) Protein engineering using molecular assembly: Functional conversion of cytochrome *c* via noncovalent interactions. *J. Am. Chem. Soc. 119*, 9096−9102.
(74) Ying, T., Wang, Z. H., Lin, Y. W., Xie, J., Tan, X., and Huang, Z. X. (2009) Tyrosine-67 in cytochrome *c* is a possible apoptotic trigger controlled by hydrogen bonds via a conformational transition. *Chem. Commun.*, 4512−4514.
(75) Smith, C. R., Wandschneider, E., and Bowler, B. E. (2003) Effect of pH on the iso-1 cytochrome *c* denatured state: Changing constraints due to heme ligation. *Biochemistry 42*, 2174−2184.
(76) Hanske, J. (2012) Probing cytochrome *c*-cardiolipin interactions in mitochondrial membranes: Towards a biophysical and cell biology toolbox. Diploma thesis, pp 134, Freie Universitat Berlin, Berlin.
(77) Muenzner, J. (2012) Dynamics of cytochrome *c* unfolding upon interaction with cardiolipin-containing liposomes. Bachelor's thesis, pp 102, University of Bonn, Bonn, Germany.
(78) Tsang, W. Y., and Lemire, B. D. (2003) The role of mitochondria in the life of the nematode, *Caenorhabditis elegans*. *Biochim. Biophys. Acta 1638*, 91−105.
(79) Reider, R., and Bosshard, H. (1980) Comparison of the binding sites on cytochrome *c* for cytochrome *c* oxidase, cytochrome *bc*1, and cytochrome *c*1. *J. Biol. Chem. 255*, 4732−4739.
(80) Hammack, B. N., Godbole, S., and Bowler, B. E. (1998) Cytochrome *c* folding traps are not due solely to histidine-heme ligation: Direct demonstration of a role for N-terminal amino group-heme ligation. *J. Mol. Biol. 275*, 719−724.
(81) Lo, T. P., Murphy, M. E. P., Guillemette, J. G., Smith, M., and Brayer, G. D. (1995) Replacements in a conserved leucine cluster in the hydrophobic heme pocket of cytochrome *c*. *Protein Sci. 4*, 198−208.
(82) Rytömaa, M., and Kinnunen, P. K. (1994) Evidence for two distinct acidic phospholipid-binding sites in cytochrome *c*. *J. Biol. Chem. 269*, 1770−1774.
(83) Kostrzewa, A., Pali, T., Froncisz, W., and Marsh, D. (2000) Membrane location of spin-labeled cytochrome *c* determined by paramagnetic relaxation agents. *Biochemistry 39*, 6066−6074.
(84) Arama, E., Bader, M., Srivastava, M., Bergmann, A., and Steller, H. (2006) The two *Drosophila* cytochrome *c* proteins can function in both respiration and caspase activation. *EMBO J. 25*, 232−243.
(85) Goldberg, E., Sberna, D., Wheat, T. E., Urbanski, G. J., and Margoliash, E. (1977) Cytochrome *c*: Immunofluorescent localization of the testis-specific form. *Science 196*, 1010−1012.
(86) Liu, Z., Lin, H., Ye, S., Liu, Q. Y., Meng, Z., Zhang, C. M., Xia, Y., Margoliash, E., Rao, Z., and Liu, X. J. (2006) Remarkably high activities of testicular cytochrome *c* in destroying reactive oxygen species and in triggering apoptosis. *Proc. Natl. Acad. Sci. U.S.A. 103*, 8965−8970.
(87) Kim, S. K., Lund, J., Kiraly, M., Duke, K., Jiang, M., Stuart, J. M., Eizinger, A., Wylie, B. N., and Davidson, G. S. (2001) A gene expression map for *Caenorhabditis elegans*. *Science 293*, 2087−2092.